

Long coherence of electron spins coupled to a nuclear spin bath

Hendrik Bluhm^{1*}, Sandra Foletti^{1*}, Izhar Neder¹, Mark Rudner¹, Diana Mahalu², Vladimir Umansky² & Amir Yacoby¹

¹*Department of Physics, Harvard University, Cambridge, MA 02138, USA*

²*Braun Center for Submicron Research, Department of Condensed Matter Physics, Weizmann Institute of Science, Rehovot 76100, Israel*

**These authors contributed equally to this work.*

Qubits, the quantum mechanical bits required for quantum computing, must retain their fragile quantum states over long periods of time. In many types of electron spin qubits, the primary source of decoherence is the interaction between the electron spins and nuclear spins of the host lattice. For electrons in gate defined GaAs quantum dots, previous spin echo measurements have revealed coherence times of about 1 μ s at low magnetic fields below 100 mT (ref 1, 2). Here, we show that coherence in such devices can actually survive to much longer times, and provide a detailed understanding of the measured nuclear spin induced decoherence. At fields above a few hundred millitesla, the coherence time measured using a single-pulse spin echo extends to 30 μ s. At lower magnetic fields, the echo first collapses, but then revives at later times given by the period of the relative Larmor precession of different nuclear species. This behavior was recently predicted^{3,4}, and as we show can be quantitatively accounted for by a semi-classical model for the electron spin dynamics in the presence of a nuclear spin bath. Using a multiple-pulse Carr-Purcell-Meiboom-Gill echo sequence, the decoherence time can be extended to more than 200 μ s, which represents an improvement by two orders of magnitude compared to previous measurements^{1,2,5}. This demonstration of effective methods to mitigate nuclear spin induced decoherence puts the quantum error correction threshold within reach.

The promise of quantum dot spin qubits as a solid state approach to quantum computing is demonstrated by the successful realization of initialization, control and single shot readout of electron spin qubits in GaAs quantum dots using optical⁶, magnetic⁷, and fully electrical⁸⁻¹⁰ techniques. To further advance spin based quantum computing, it is vital to mitigate decoherence due to the interaction of the electron spin with the spins of nuclei of the host material. Understanding the dynamics of this system is also of great fundamental interest^{11,12}.

Through the hyperfine interaction, an electron spin in a GaAs quantum dot is subjected to an effective magnetic field produced by the nuclear spins. Under typical experimental conditions, this so-called ‘‘Overhauser field’’ has a random magnitude and direction. Typically, measurements of the coherent electron spin precession involve averaging over many experimental runs, and thus over many Overhauser field configurations. As a result, the coherence signal is suppressed for evolution times $\tau \gtrsim T_2^* \approx 10$ ns (ref 1). However, the nuclear spins evolve much more slowly

than the electron spins, so that the Overhauser field is nearly static for a sufficiently short duration of electron spin evolution. Therefore, it is possible to partially eliminate the effect of the random nuclear field by flipping the electron spin halfway through an interval of free precession¹³, a procedure known as Hahn-echo. The random contributions of the Overhauser field to the electron spin precession before and after the spin-reversal then approximately cancel out. For longer evolution times, the effective field acting on the electron spin generally changes between the two halves of the precession interval. This change leads to an eventual loss of coherence on a time scale determined by the details of the nuclear spin dynamics.

Previous Hahn-echo experiments in GaAs quantum dot spin qubits have demonstrated spin dephasing times of around 1 μ s at relatively low magnetic fields up to 100 mT (ref 1, 2). Recent theoretical studies of decoherence due to the hyperfine interaction^{3,4,14} are generally consistent with these experimental results, but predict revivals of the echo signal after several microseconds, as also seen in other systems¹⁵. This prediction already indicates that the initial decay of the echo does not reflect irreversible decoherence, but is a consequence of the coherent Larmor precession of the nuclei. Theoretical work also predicted much longer coherence times at higher external magnetic fields¹⁶ or when using more advanced pulse sequences^{17,18}. The classic example is the Carr-Purcell-Meiboom-Gill (CPMG) sequence^{1,19}, but several alternatives have recently been developed^{20,21} and demonstrated^{22,23}. The performance of such schemes is expected to improve as more control pulses are added¹⁸. Here, we provide direct experimental confirmations for all the above predictions.

The spin qubit studied in this work consists of two isolated electrons confined in a double quantum dot, created by applying negative voltages to metallic gates that locally deplete a two dimensional electron gas (2DEG) 90 nm below the wafer surface (see Fig. 1a). The Hilbert space of our logical qubit is spanned by the states $|\uparrow\downarrow\rangle$ and $|\downarrow\uparrow\rangle$, i.e. the $m = 0$ subspace of two separated spins. The arrows represent the alignment of the electron spins in each of the dots relative to an external magnetic field, B_{ext} , which is oriented in the plane of the 2DEG. The remaining two states, $T_+ \equiv |\uparrow\uparrow\rangle$ and $T_- \equiv |\downarrow\downarrow\rangle$, are energetically separated by the Zeeman energy $E_Z = g^* \mu_B B_{ext}$ ($g^* = -0.44$ is the g -factor in GaAs) and are not used for information storage. Tunnel coupling to the leads is used for initialization, while inter-dot tunnel coupling allows spin exchange between the dots. This exchange interaction is modulated via the detuning ε , which is the difference between the electrostatic potentials in the two dots. This parameter is controlled via rapid, antisymmetric changes of the voltages on gates GL and GR (see Fig. 1) applied via high frequency coaxial lines, which enables fast electrical control of the qubit^{1,8,24}

The experimental procedures follow those of ref 1. We initialize the system at a large detuning, where the ground state is a spin singlet with both electrons residing in a single dot. As ε is swept to negative values, the electrons separate into different dots, thus preparing the singlet state $S \equiv (|\uparrow\downarrow\rangle - |\downarrow\uparrow\rangle)/\sqrt{2}$. For very large negative detunings, the electron spins in the two dots are decoupled, and each individually experiences a Zeeman field composed of the homogeneous external field and a fluctuating local hyperfine field. A difference ΔB_{nuc}^z between the z -components of the

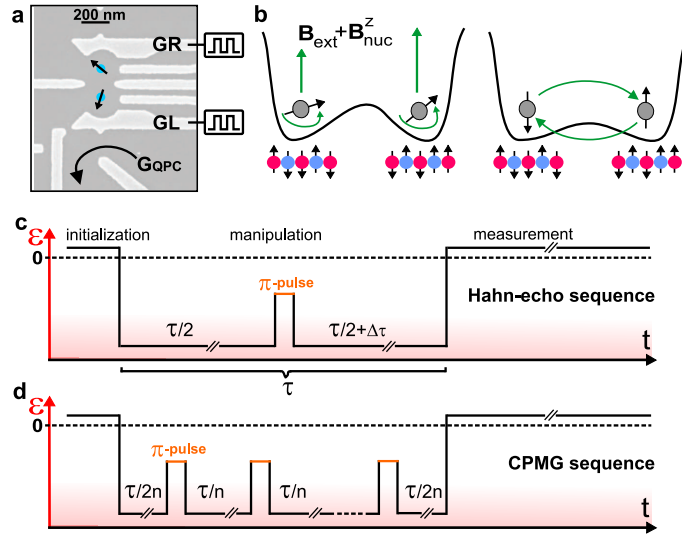


Figure 1: **Qubit control.** **a**, SEM micrograph of a device similar to the one used. Metal gates (bright structures) are negatively biased to confine two electrons. The charge state of the double quantum dot is determined by measuring the conductance through the capacitively coupled quantum point contact, G_{QPC} . The separation between the two electrons is controlled with nanosecond time resolution via the voltages on GR and GL. **b**, Left: an initially prepared singlet state oscillates between S and T_0 with frequency $g^* \mu_B \Delta B_{\text{nuc}}^z / \hbar$, which changes over time due to slow fluctuations of the hyperfine field gradient ΔB_{nuc}^z . Right: switching on the tunnel coupling between the two dots leads to the coherent exchange of the electron spins. **c**, Hahn-echo sequence: after evolving for a time $\tau/2$, the two electrons are exchanged with a π -pulse. The singlet state is recovered after further evolution for another $\tau/2$, independent of ΔB_{nuc}^z . **d**, Carr-Purcell-Meiboom-Gill sequence: in this higher order decoupling sequence, n π -pulses at time intervals τ/n are applied.

hyperfine fields in the two dots leads to an energy splitting between the basis states $|\uparrow\downarrow\rangle$ and $|\downarrow\uparrow\rangle$. This splitting causes precession between the singlet S and the triplet $T_0 \equiv (|\uparrow\downarrow\rangle + |\downarrow\uparrow\rangle)/\sqrt{2}$, and its fluctuations lead to dephasing of the qubit. We implement the echo π -pulses by pulsing to small negative detunings, where inter-dot tunneling leads to an exchange splitting between S and T_0 . This splitting drives coherent oscillations between the states $|\uparrow\downarrow\rangle$ and $|\downarrow\uparrow\rangle$. The pulse profiles for the Hahn-echo and CPMG sequence are shown in Fig. 1c,d.

Readout of the final qubit state is accomplished by switching to positive detuning, $\varepsilon > 0$, where the state with both electrons sitting in the same dot is preferred for the spin singlet, but is energetically excluded for a spin-triplet due to the Pauli exclusion principle. The two spin states thus acquire different charge densities. To sense this difference, we use a proximal quantum point contact (QPC), whose conductance depends on the local electrostatic environment²⁵. After averaging over many identical pulse cycles, the mean QPC conductance, G_{QPC} , reflects the probability to find the qubit in the singlet state at the end of each cycle. The echo amplitudes presented below are normalized such that they are unity at short times (no decoherence) and eventually drop to zero for a fully randomized state. This normalization eliminates τ -independent contrast losses (see Supplementary Material). Fig. 2a shows the Hahn-echo signals for different magnetic fields B_{ext} .

At high fields we find a monotonic decay of the Hahn-echo signal with the total duration of free precession, τ . The echo initially decays very slowly (approximately proportional to τ^4), and is suppressed to $1/e$ after $30 \mu\text{s}$. As the magnetic field is reduced, the echo signal develops oscillations with a time scale of microseconds. For even lower fields, the oscillations evolve into full collapses of the signal, with revivals at later times on a ten microsecond time scale. These revivals were predicted in refs 3, 4 based on a quantum mechanical treatment of the hyperfine interaction between electron and nuclear spins. Below we outline a semiclassical model²⁶ that can reproduce the lowest-order result of refs 3, 4 and accounts for additional effects that are essential for fitting our data. This model provides the theoretical echo signal, $C(\tau) \equiv 2p(S) - 1 = -\text{Re}\langle\uparrow\downarrow|\rho(\tau)|\downarrow\uparrow\rangle$, where $p(S)$ is the probability of finding the electron in a singlet state and $\rho(\tau)$ is the qubit's density matrix at the end of the evolution time. We have used this model to produce the quantitatively accurate fits displayed in Fig. 2a.

For each electron spin, the Zeeman energy splitting is proportional to the total magnetic field $B_{tot} = \sqrt{(B_{ext} + B_{nuc}^z)^2 + B_{nuc}^\perp{}^2} \approx B_{ext} + B_{nuc}^z + B_{nuc}^\perp{}^2/2B_{ext}$ (Fig. 2b). Time-dependence of the parallel and transverse nuclear components, B_{nuc}^z and $B_{nuc}^\perp{}^2$, can lead to dephasing of the electron spin. Assuming statistical independence between B_{nuc}^z and $B_{nuc}^\perp{}^2$, the theoretical echo signal can be written as a product, $C(\tau) = A_z(\tau)R_\perp(\tau)$, where $A_z(\tau)$ and $R_\perp(\tau)$ account for the contributions of B_{nuc}^z and $B_{nuc}^\perp{}^2$ to the electron spin precession. In the experimental range of the magnetic fields, the time-dependence of B_{nuc}^z is mainly caused by spectral diffusion due to the dipole-dipole interaction between nuclear spins. This process is predicted to lead to a decay of the form $A_z(\tau) = \exp(-(\tau/T_{SD})^4)$ (ref 14, 16). As we will now discuss, $R_\perp(\tau)$ (see Supplementary Eq. 1) has a more interesting non-monotonic structure which arises from the relative precession of

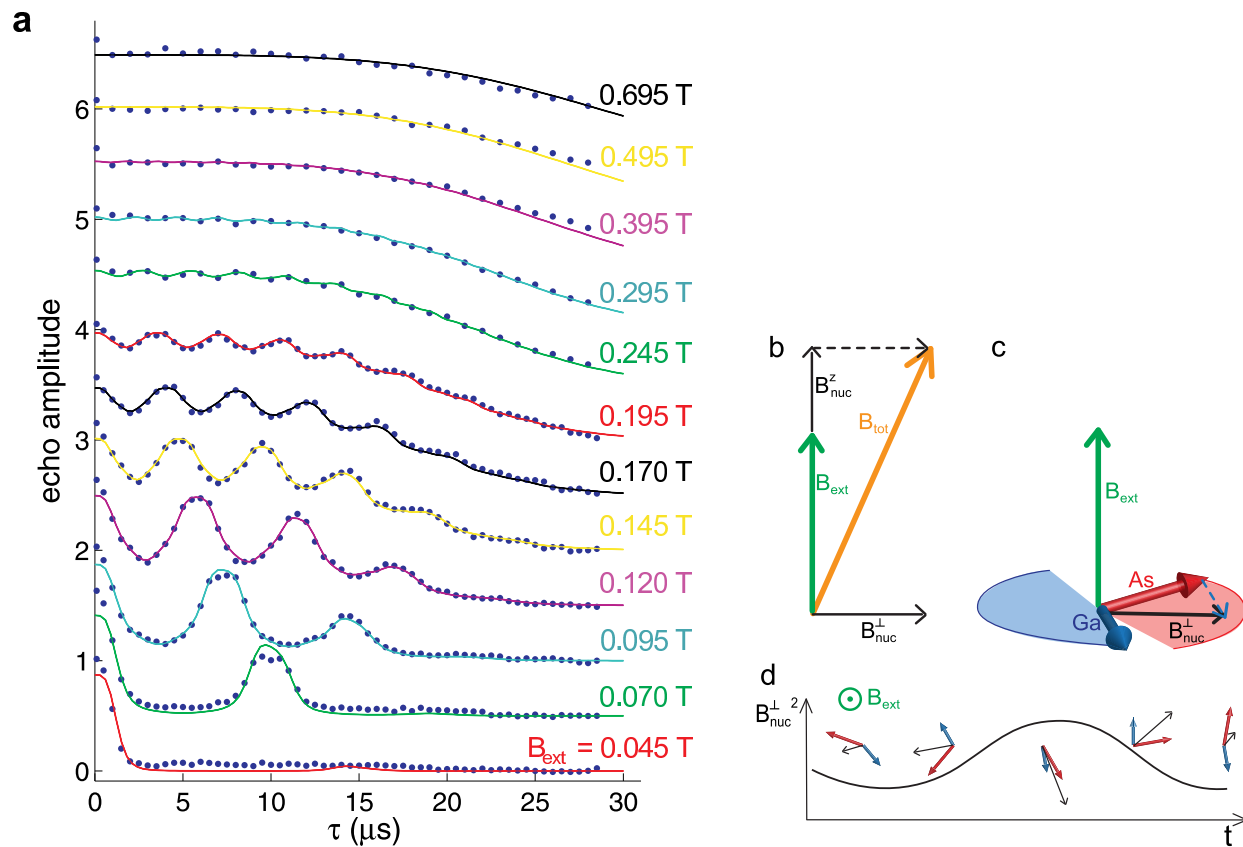


Figure 2: **Echo amplitude.** **a**, Echo signal as a function of the total evolution time, τ , for different values of magnetic field. The fits to the data are obtained by extending the model of ref 3 to include a spread δB_{loc} of the nuclear Larmor frequencies²⁶ and multiplying with $\exp((-\tau/T_{SD})^4)$. Curves are offset for clarity and normalized as discussed in the Supplementary Material. **b**, The total Zeeman field seen by the electron is the vector sum of the external field and the Overhauser fields parallel and perpendicular to it. **c**, The three nuclear species (only two shown for clarity) contributing to the Overhauser field precess at different Larmor frequencies in the external field. **d**, As a result of the relative precession (top), the total transverse nuclear field oscillates at the Larmor frequency difference(s) (bottom).

nuclear spins in the external field with different Larmor frequencies.

The transverse hyperfine field, $\vec{B}_{\text{nuc}}^\perp$, is a vector sum of contributions from the three nuclear species ^{69}Ga , ^{71}Ga and ^{75}As . Due to the different precession rates of these species (Fig. 2c), $B_{\text{nuc}}^\perp(t)^2$ contains harmonics at the three relative Larmor frequencies (Fig. 2d) in addition to a constant term. The contribution of the constant term to the singlet return probability is eliminated by the echo pulse. For a general free precession period, the time-dependence leads to a suppression of the echo signal. However, if the precession interval $\tau/2$ is a multiple of all three relative Larmor periods, the oscillatory components contribute no net phase to the electron spin evolution. As a result, the echo amplitude revives whenever the commensurability condition is met. Averaging the singlet return probability over initial Overhauser field configurations²⁶ leads to the collapse-and-revival behavior predicted in refs 3,4.

At low fields, the echo envelope decays more quickly than at high fields (see Fig. 2a). This field dependence can be accounted for by including a spread of the Larmor precession frequencies for each nuclear species. Such a variation is also manifest in the width of NMR lines and naturally arises from dipolar and other interactions between nuclei²⁷. We model it as a shift of the magnetic field acting on each individual nuclear spin by an amount B_{loc} , where B_{loc} is a Gaussian random variable with standard deviation δB_{loc} . This spread of precession frequencies leads to an aperiodic time-dependence of B_{nuc}^\perp , which cannot be removed by the electron spin echo.

Using the above model (see also Supplementary Eq. 1), we have fit all the data in Fig. 2a with a single set of field-independent parameters which were chosen to obtain a good match with all datasets: the number of nuclei in each of the two dots, N , the spectral diffusion time constant, T_{SD} , and δB_{loc} . In addition, the scale factor for each dataset was allowed to vary to account for the imperfect normalization of the data. The value of N determines the depths of the dips between revivals. The best fit yields $N = 4.4 \times 10^6$, which is in good agreement with an independent determination from a measurement of $T_2^* = \sqrt{N}\hbar/g^*\mu_B \cdot 4.0 \text{ T}$ giving $N = 4.9 \times 10^6$ (see ref 28, Supplementary Material). From the fit we also obtain $T_{SD} \approx 37 \mu\text{s}$ and $\delta B_{\text{loc}} = 0.3 \text{ mT}$. The measured NMR line width in pure GaAs is about 0.1 mT (ref 27). A possible origin for the larger field inhomogeneity found here is the quadrupole splitting arising from the presence of the two localized electrons²⁹. The inhomogeneity of the Knight shift is expected to have a similar but quantitatively negligible effect for our parameters. The value of T_{SD} is consistent with theoretical estimates (see Supplementary Material and ref 16). Interestingly, the spread of nuclear Larmor frequencies, captured by δB_{loc} , contributes significantly to the echo decay even at the highest fields investigated. We have also verified that the Hahn-echo lifetime is not significantly affected by dynamic nuclear polarization, which can be used to increase T_2^* (ref 30, Supplementary Material).

In order to measure the long Hahn-echo decay times of up to 30 μs , it was necessary to systematically optimize the pulses (see Supplementary Material). Small differences in the gate

voltages before and after the π -pulse shift the electronic wave function relative to the inhomogeneously polarized nuclei. Such shifts cause the electrons to sample different Overhauser fields at different times, and thus lead to an imperfect echo. We have minimized this effect by compensating for a systematic drift of ε over the course of each pulse sequence (see Supplementary Material).

Substantially longer coherence times are expected for more elaborate decoupling sequences¹⁸. We implemented the CPMG sequence¹⁹, which consists of an n -fold repetition of the Hahn-echo, thus requiring n π -pulses, as shown in Fig. 1d. Fig. 3 shows data for $n = 6, 10$ and 16 . For $n = 16$, the echo signal clearly persists for more than $200 \mu\text{s}$. The field dependence for $n = 4$ is reported in the Supplementary Material. To verify the interpretation of the data, we have measured the dependence of the echo on small changes in the final free precession time and the duration of the exchange pulses for $n = 10$, $\tau = 5$ and $120 \mu\text{s}$ (Supplementary Material). Because of the large number of potential tuning parameters, we have not optimized these CPMG pulses. We expect that with improved pulses, the same extension of the coherence time could be achieved with fewer pulses. The linear initial decay of the signal in Fig. 3 is not well understood. The similar variation of the reference signal corresponding to a completely mixed state is suggestive of a single-electron T_1 process causing leakage into the T^+ and T^- states (see Supplementary Material). The decay time constant sets a lower bound for the largest achievable coherence time.

Our measurements demonstrate coherence times of GaAs spin qubits of at least $200 \mu\text{s}$, two orders of magnitude larger than previously shown. The duration of each of the π -pulses could easily be reduced below the 6 ns used here. Thus, more than 10^5 operations could be carried out within the coherence time, well in excess of the commonly quoted error correction threshold of $\sim 10^4$. Furthermore, one may hope to achieve millisecond scale coherence times with improved decoupling sequences¹⁸ without adding complexity. The excellent agreement with the model for the field and time dependence of the Hahn-echo revivals shows that many aspects of the dephasing of electron spins due to the nuclear hyperfine interaction are now well understood. The insight gained may also help pave the way towards probing macroscopic quantum effects in a mesoscopic ensemble of a few million nuclear spins.

1. Petta, J. R. *et al.* Coherent manipulation of coupled electron spins in semiconductor quantum dots. *Science* **309**, 2180 (2005).
2. Koppens, F. H. L., Nowack, K. & Vandersypen, L. M. K. Spin echo of a single spin in a quantum dot. *Phys. Rev. Lett.* **100**, 236802 (2008).
3. Cywinski, L., Witzel, W. M. & Das Sarma, S. Pure quantum dephasing of a solid-state electron spin qubit in a large nuclear spin bath coupled by long-range hyperfine mediated interactions. *Phys. Rev. B* **79**, 245314 (2009).
4. Cywinski, L., Witzel, W. M. & Das Sarma, S. Electron spin dephasing due to hyperfine interactions with a nuclear spin bath. *Phys. Rev. Lett.* **102**, 057601 (2009).

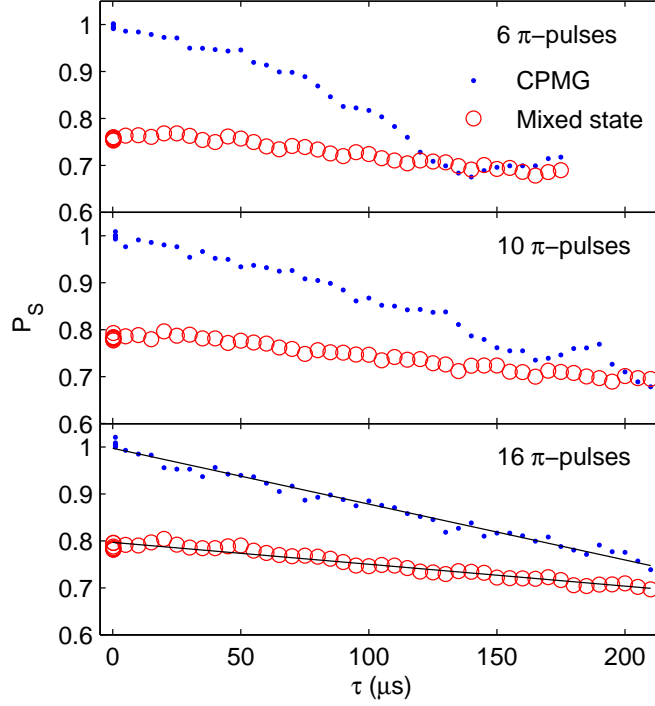


Figure 3: **CPMG decoupling experiments with 6, 10 and 16 π -pulses** at $B_{ext} = 0.4$ T. The blue dots show the readout signal of the CPMG pulses, the red circles represent reference measurements with the same evolution time without any π -pulses (equivalent to T_2^* measurements), which produce a completely dephased state. P_S is the sensor signal normalized by the DC contrast associated with the transfer of an electron from one dot to the other, so that a singlet corresponds to $P_S = 1$ (See Supplementary Material). Inelastic decay during the readout phase and possibly other visibility loss mechanisms increase P_S for the mixed state above the ideal value of 0.5. The linear trends in the reference and the initial decay of the CPMG signal likely reflect leakage out of the logical subspace. The linear fits to the 16-pulse data (black lines) intersect at $\tau = 276 \mu s$, which can be taken as a rough estimate or lower bound of the coherence time.

5. Greilich, A. *et al.* Mode locking of electrons spin coherence in singly charged quantum dots. *Science* **313**, 341 (2006).
6. Press, D., Ladd, T., Zhang, B. & Yamamoto, Y. Complete quantum control of a single quantum dot spin using ultrafast optical pulses. *Nature* **456**, 218 (2008).
7. Koppens, F. H. L. *et al.* Control and detection of singlet-triplet mixing in a random nuclear field. *Science* **309**, 1346 (2005).
8. Foletti, S., Bluhm, H., Mahalu, D., Umansky, V. & Yacoby, A. Universal quantum control in two-electron spin quantum bits using dynamic nuclear polarization. *Nature Physics* **5**, 903 (2009).
9. Nowack, K. C., Koppens, F. H. L., Nazarov, Y. V. & Vandersypen, L. M. K. Coherent control of a single electron spin with electric fields. *Science* **318**, 1430 (2007).
10. Barthel, C., Reilly, D. J., Marcus, C. M., Hanson, M. P. & Gossard, A. C. Rapid single-shot measurement of a singlet-triplet qubit. *Phys. Rev. Lett.* **103**, 160503 (2009).
11. Coish, W. A., Fischer, J. & Loss, D. Exponential decay in a spin bath. *Phys. Rev. B.* **77**, 125329 (2008).
12. Chen, G., Bergman, D. L. & Balents, L. Semiclassical dynamics and long-time asymptotics of the central-spin problem in a quantum dot. *Phys. Rev. B* **76**, 045312 (2007).
13. Hahn, E. L. Spin echoes. *Phys. Rev.* **80**, 580 (1950).
14. Yao, W., Liu, R. B. & Sham, L. J. Theory of electron spin decoherence by interacting nuclear spins in a quantum dot. *Phys. Rev. B.* **74**, 195301 (2006).
15. Childress, L. *et al.* Coherent dynamics of coupled electron and nuclear spin qubits in diamond. *Science* **314**, 281 (2006).
16. Witzel, W. M. & Sarma, S. D. Quantum theory for electron spin decoherence induced by nuclear spin dynamics in semiconductor quantum computer architecture. *Phys. Rev. B.* **74**, 035322 (2006).
17. Witzel, W. M. & Das Sarma, S. Multiple-pulse coherence enhancement of solid state spin qubits. *Phys. Rev. Lett.* **98**, 077601 (2007).
18. Lee, B., Witzel, W. M. & Sarma, S. D. Universal pulse sequence to minimize spin dephasing in the central spin decoherence problem. *Phys. Rev. Lett.* **100**, 160505 (2008).
19. Meiboom, S. & Gill, D. Modified spin-echo method for measuring nuclear relaxation times. *Rev. Sci. Inst.* **29**, 688 (1958).
20. Khodjasteh, K. & Lidar, D. A. Performance of deterministic dynamical decoupling schemes: Concatenated and periodic pulse sequences. *Phys. Rev. A* **75**, 062310 (2007).

21. Uhrig, G. S. Keeping a quantum bit alive by optimizing π -pulse sequences. *Phys. Rev. Lett.* **98**, 100504 (2007).
22. Biercuk, M. J. *et al.* Optimized dynamical decoupling in a model quantum memory. *Nature* **458**, 996–1000 (2009).
23. Du, J. *et al.* Preserving electron spin coherence in solids by optimal dynamical decoupling. *Nature* **461**, 1265–1268 (2009).
24. Levy, J. Universal quantum computation with spin-1/2 pairs and heisenberg exchange. *Phys. Rev. Lett.* **89**, 147902 (2002).
25. Field, M. *et al.* Measurements of coulomb blockade with a noninvasive voltage probe. *Phys. Rev. Lett.* **70**, 1311 (1993).
26. Neder, I., Rudner, M., Bluhm, H. & Yacoby, A. Semi-classical model for dephasing of an electron spin qubit coupled to a nuclear spin bath. (to be published).
27. Sundfors, R. K. Exchange and quadrupole broadening of nuclear acoustic resonance line shapes in the III-V semiconductors. *Phys. Rev.* **185**, 458–472 (1969).
28. Taylor, J. M. *et al.* Relaxation, dephasing, and quantum control of electron spins in double quantum dots. *Phys. Rev. B.* **76**, 035315 (2007).
29. Hester, R. K., Sher, A., Soest, J. F. & Weisz, G. Nuclear-magnetic-resonance detection of charge defects in gallium arsenide. *Phys. Rev. B* **10**, 4262–4273 (1974).
30. Bluhm, H., Foletti, S., Mahalu, D., Umansky, V. & Yacoby, A. Enhancing the coherence of spin qubits by narrowing the nuclear spin bath with a quantum feedback loop (2010). (submitted to PRL), [arXiv:1003.4031](https://arxiv.org/abs/1003.4031).

Acknowledgments We thank D. J. Reilly for advice on implementing the RF readout system and Jero Maze for discussions. We acknowledge funding from ARO/IARPA, the Department of Defense and the National Science Foundation under award number 0653336. I.N. and M.R. were supported by NSF grant DMR-0906475. This work was performed in part at the Center for Nanoscale Systems (CNS), a member of the National Nanotechnology Infrastructure Network (NNIN), which is supported by the National Science Foundation under NSF award no. ECS-0335765.

Author Contributions e-beam lithography and MBE growth were carried out by D.M. and V.U., respectively. H.B., S.F. and A.Y. fabricated the sample, planned and executed the experiment and analyzed the data. I.N., M.R. and H.B. and A.Y. developed the theoretical model. H.B., S.F. and A.Y., I.N. and M.R. wrote the paper.

Correspondence Correspondence and requests for materials should be addressed to A.Y. (email: yacoby@physics.harvard.edu).